APL Materials

A substantial increase of Curie temperature in a new type of diluted magnetic semiconductors via effects of chemical pressure

Shuang Yu, Guoqiang Zhao (iD), Yi Peng, Xiaohong Zhu, Xiancheng Wang, Jianfa Zhao, Lipeng Cao, Wenmin Li, Zhi Li, Zheng Deng (iD), and Changqing Jin

View Online   Export Citation   CrossMark

ARTICLES YOU MAY BE INTERESTED IN

A substantial increase of Curie temperature in a new type of diluted magnetic semiconductors via effects of chemical pressure

View Online   Export Citation   CrossMark

Shuang Yu,[1,2] Guoqiang Zhao,[1,2] (ID) Yi Peng,[1,3] Xiaohong Zhu,[3] Xiancheng Wang,[1,2] Jianfa Zhao,[1,2] Lipeng Cao,[1,2] Wenmin Li,[1,2] Zhi Li,[4,a] Zheng Deng,[1,2,b] (ID) and Changqing Jin[1,2,5,c]

AFFILIATIONS

[1] Beijing National Laboratory for Condensed Matter Physics, and Institute of Physics, Chinese Academy of Sciences, Beijing 100190, China

[2] School of Physics, University of Chinese Academy of Sciences, Beijing 100190, China

[3] Department of Materials Science and Engineering, Sichuan University, Chengdu, China

[4] School of Materials Science and Engineering, Nanjing University of Science and Technology, 210094 Nanjing, China

[5] Materials Research Lab at Songshan Lake, 523808 Dongguan, China

[a] Electronic mail: zhili@njust.edu.cn
[b] Electronic mail: dengzheng@iphy.ac.cn
[c] Electronic mail: Jin@iphy.ac.cn

ABSTRACT

Chemical pressure is an effective method to tune physical properties, particularly for diluted magnetic semiconductors (DMSs) of which ferromagnetic ordering is mediated by charge carriers. Via substitution of smaller Ca for larger Sr, we introduce chemical pressure on $(Sr,Na)(Cd,Mn)_2As_2$ to fabricate a new DMS material $(Ca,Na)(Cd,Mn)_2As_2$. Carriers and spins are introduced by substitutions of (Ca,Na) and (Cd,Mn), respectively. The unit cell volume reduces by 6.2% after complete substitution of Ca for Sr, suggesting a subsistent chemical pressure. Importantly, the local geometry of the $[Cd/MnAs_4]$ tetrahedron is optimized via chemical compression that increases the Mn–As hybridization leading to enhanced ferromagnetic interactions. As a result, the maximum Curie temperature (T_C) is increased by about 50% while the maximum saturation moment increases by over 100% from $(Sr,Na)(Cd,Mn)_2As_2$ to $(Ca,Na)(Cd,Mn)_2As_2$. The chemical pressure estimated from the equation of state is equal to an external physical pressure of 3.6 GPa.

The diluted magnetic semiconductors (DMSs) have been investigated extensively as they offer an opportunity to control the ferromagnetic properties by changing carrier density. The advantage leads to potential applications in spintronic devices.[1–3] Specifically, recently couples of Fe-doped III–V DMS reached relatively high Curie temperature,[4–6] which challenges existing concepts and motivates further understanding of ferromagnetism in DMS. The spin and charge doping are induced by one element doping such as Mn doping into (Ga,Mn)As leading to difficulty in tuning either conducting or magnetic properties.[7] Consequently, a series of a new type of DMS materials with independent carrier and spin doping

have been discovered to overcome aforementioned difficulty, e.g., $Li_{1+x}(Zn,Mn)As$ termed "111" type or $(Ba,K)(Zn,Mn)_2As_2$ (BZA) termed "122" type. BZA holds the record of Curie temperature among the "111" and "122"-type DMSs.[7–11]

Given a DMS material, effective ways to modify T_C can be achieved by increasing the carrier density using an applied electric field, photoexcitations, or pressure.[7,12] Particularly, pressure is expected to increase both carrier concentration and Mn–As hybridization which result in an enhancement of ferromagnetic interactions in DMS materials.[13] On the other hand, internal chemical pressure, which plays a comparable role as external

physical pressure, is widely used to modify physical properties in many functional materials. For instance, an equivalent increase in superconducting critical temperature in cuprate superconductors has been reported via relatively low pressures (4–6 GPa) induced by chemical pressure.[14,15] Superconductivity in the iron-based compound $BaFe_2As_2$ can be induced by moderate pressure (<6 GPa) and isovalent chemical doping ($BaFe_2As_{2-x}P_x$), respectively.[16,17] Comparing to external physical pressure, internal chemical pressure, which can be applied by isovalent substitutions, does not require any specific devices (e.g., diamond anvil cell or piston cylinder cell). Nevertheless, chemical pressure-effects in DMS materials are rarely reported.

Previous studies of physical pressure-effects on "122" BZA only presented negative pressure-effect on T_C. The proposed reason is that physical pressure distorts [MnAs$_4$] tetrahedra and then reduces effective Mn–As hybridization which in turn damages ferromagnetic ordering.[18–20] In this work, we generated chemical pressure by changing atom size on another group of DMS $(Sr,Na)(Cd,Mn)_2As_2$.[21] Replacing Sr by Ca, $(Ca,Na)(Cd,Mn)_2As_2$ was synthesized as a new DMS material. From Sr- to Ca-compound, the unit cell volume decreases by 6.2% suggesting positive chemical pressure effect. It is found that local geometry of [MnAs$_4$] tetrahedron in $(Ca,Na)(Cd,Mn)_2As_2$ is optimized by chemical pressure. Consequently, a successful improvement of ferromagnetic ordering by chemical pressure has been observed: comparing to $(Sr,Na)(Cd,Mn)_2As_2$, both maximum Curie temperature and saturation moment in $(Ca,Na)(Cd,Mn)_2As_2$ are significantly enhanced.

Polycrystalline samples of $(Ca,Na)(Cd,Mn)_2As_2$ were synthesized by solid state reaction with high purity elements. The stoichiometric ratios of starting materials were well mixed and pressed into pellets. All the processes were conducted under the protection of high-purity argon due to the air-sensitive starting materials. The pellets were sealed in tantalum-tubes with 1 bar of argon, and then the Ta-tubes were enclosed into evacuated quartz tubes. The samples were first heated at 600 °C for 12 h. Then, the products were reground, pelleted, and sintered at 650 °C for another 12 h. The recovered samples were characterized by powder X-ray diffraction (PXRD) with a Rigaku diffractometer using Cu-Kα radiation at room-temperature. A Scanning Electron Microscope (SEM) was used to investigate the morphology and particle size. Real compositions of all the elements were measured with energy dispersive X-ray (EDX) analysis on the SEM. The real atom ratios of our samples are consistent with their normal stoichiometry. For example, the real composition of nominal $(Ca_{0.95}Na_{0.05})(Cd_{0.95}Mn_{0.05})_2As_2$ is determined as $(Ca_{0.9546}Na_{0.0454})(Cd_{0.9396}Mn_{0.0604})_2As_2$. Consequently, we use normal composition of each sample in this manuscript, for the sake of simplification. The dc magnetic properties were measured with a Superconductivity Quantum Interference Device (SQUID, Quantum Design), and transport properties were examined by Physical Property Measurement System (PPMS, Quantum Design). We calculated the equation of state (EoS) by first-principles calculations with a plane augmented-wave (PW) pseudopotential and generalized gradient approximation implemented in the VASP code with $16 \times 16 \times 8$ k-point grid and 500 eV energy cutoff to build up relationship between cell volume and pressure [$P(V)$] of $SrCd_2As_2$.

Both $CaCd_2As_2$ and $SrCd_2As_2$ crystallize into a hexagonal structure with P-$3m1$ space group (No. 164) as shown in Fig. 1(a). Powder X-ray diffraction patterns for samples show that all of the peaks can be well indexed into P-$3m1$ space group (Fig. S1). For all the samples, crystal grains have sharp boundaries indicating good
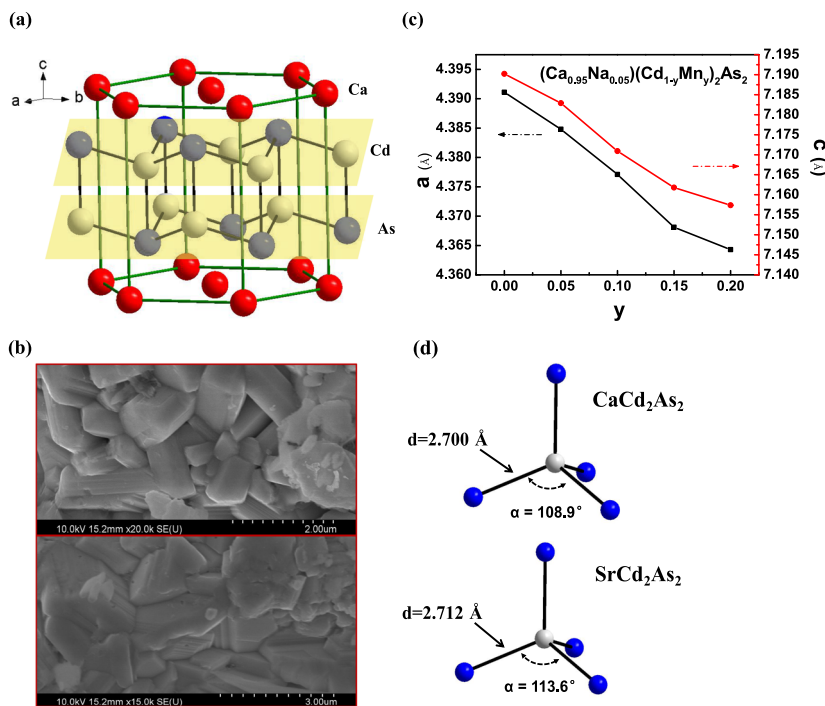
FIG. 1. (a) Crystal structure of the parent phase, $CaCd_2As_2$. The CdAs sublayers are highlighted with yellow parallelograms. (b) SEM images of $(Ca_{0.95}Na_{0.05})(Cd_{0.9}Mn_{0.1})_2As_2$. (c) Lattice constants vs Mn doping levels. (d) [Cd/MnAs]$_4$ tetrahedra in $(Ca_{0.95}Na_{0.05})(Cd_{0.95}Mn_{0.05})As_2$ and $(Sr_{0.95}Na_{0.05})(Cd_{0.95}Mn_{0.05})As_2$. Marked bond length and bond angle are the ones within the CdAs sublayers.

crystallization, as shown in Fig. 1(b). The lattice constants were calculated by Rietveld refinement. Both of a-axis and c-axis shrink linearly with increasing Mn doping level as shown in Fig. 1(c) because Mn^{2+} (0.66 Å) is smaller than Cd^{2+} (0.78 Å), well following the Vegard law, an evidence of successful (Cd,Mn) substitution. $CaCd_2As_2$ and $SrCd_2As_2$ are quasi-2D-materials where Ca/Sr ions layers and honeycomblike Cd_2As_2 layers stack alternately along the c axis.[22] Given lattice constants for $SrCd_2As_2$ ($a \sim 4.4516$ Å, $c \sim 7.4221$ Å, $V \sim 127.4$ Å³) and $CaCd_2As_2$ ($a \sim 4.3909$ Å, $c \sim 7.1870$ Å, $V \sim 120.0$ Å³), chemical compression effect is visible in the latter, particularly along the c-axis. Besides, two more principal deviations between $CaCd_2As_2$ and $SrCd_2As_2$ are the Cd/Mn–As bond lengths and As–Cd/Mn–As bond angles in Cd_2As_2 layers which will be discussed in more details.

Figure 2(a) shows temperature dependent of magnetization [$M(T)$] curves for $(Ca_{1-x}Na_x)(Cd_{1-y}Mn_y)_2As_2$ (x = 0.025, 0.05, 0.1, 0.15; y = 0.05, 0.15, 0.2) under field H = 500 Oe. There is no obvious difference between zero field cooling (ZFC) and field cooling (FC), but clear ferromagnetic signatures are observed for all samples, i.e., sharp upturns with decreasing temperature. T_C were determined from valleys of dM/dT curves. Above T_C, susceptibility is fitted with the Curie-Weiss law [inset of Fig. 2(a)], $(\chi - \chi_0)^{-1} = (T - \theta)/C$, where χ_0 stands for a temperature-independent

term and θ stands for paramagnetic temperature. Neither T_C nor θ monotonically increases with increasing Mn or Na doping level [Fig. 2(c)]. Maximum $T_C \sim 19$ K and $\theta \sim 22$ K are obtained for x = 0.05 and y = 0.15. The maximum T_C of (Ca,Na)(Cd,Mn)$_2$As$_2$ is about 50% higher than that of (Sr,Na)(Cd,Mn)$_2$As$_2$ (the maximum $T_C \sim 13$ K).[21] In Fig. 2(c), Tc decreases slightly with a higher Na-doping level when x > 0.05, presumable due to more defects induced by Na doping in specimens. After reaching maximum T_C, ferromagnetic ordering is also weakened by overdoped Mn, similar to analogs (Sr,Na)(Zn,Mn)$_2$As$_2$ and (Sr,Na)(Cd,Mn)$_2$As$_2$.[21,23] A presumably reason is that increasing chemical substitution tends to enhance antiferromagnetic coupling between either substitutional Mn and interstitial Mn or substitutional Mn in the nearest neighbor Cd sites due to high Mn concentration. Effective paramagnetic moments (M_{eff}) are calculated from the Curie constant C. For example, M_{eff} of (Ca$_{0.95}$Na$_{0.05}$)(Cd$_{0.95}$Mn$_{0.05}$)$_2$As$_2$ is 5.3μ_B/Mn which is close to an expected value of s = 5/2 configuration of Mn^{2+} [$g\sqrt{s(s+1)}$ = 5.9μ_B with g = 2]. Ferromagnetic characteristics, which are spontaneous magnetization under very low fields and narrow but clear hysteresis loops, are also found in $M(H)$ curves as plotted in Fig. 2(b). Coercive fields are smaller than 100 Oe. Saturation moments (M_{sat}) decrease with increasing Mn [Fig. 2(d)] due to increased antiferromagnetic interactions as proposed to explain the decrease
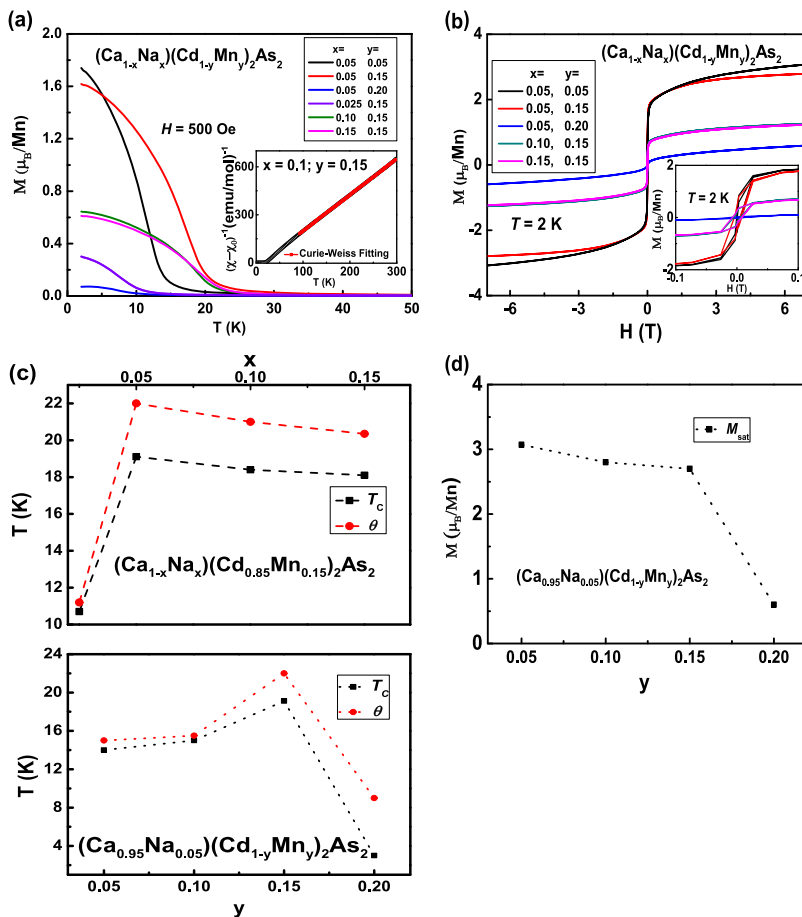
FIG. 2. (a) $M(T)$ measured under H = 500 Oe of (Ca$_{1-x}$Na$_x$)(Cd$_{1-y}$Mn$_y$)$_2$As$_2$ (x = 0.025, 0.05, 0.1, 0.15; y = 0.05, 0.15, 0.2). (b) The hysteresis loops at 2 K for (Ca$_{1-x}$Na$_x$)(Cd$_{1-y}$Mn$_y$)$_2$As$_2$ (x = 0.025, 0.05, 0.1, 0.15; y = 0.05, 0.15, 0.2). (c) T_C and θ vs Na- and Mn-doping level. (d) M_{sat} vs Mn doping level.

in T_C. Nevertheless, maximum M_{sat} of (Ca,Na)(Cd,Mn)$_2$As$_2$ is significant larger than that of (Sr,Na)(Cd,Mn)$_2$As$_2$ (maximum $M_{sat} < 1\mu_B$/Mn). The larger M_{sat} indicates that more local spins on Mn are ferromagnetic ordered, consistent with higher T_C in (Ca,Na)(Cd,Mn)$_2$As$_2$.[21]

Electrical transport measurements are shown in Fig. 3. The temperature dependent resistivity [$\rho(T)$] for parent compound CaCd$_2$As$_2$ shows semiconducting behavior within a temperature range of 2–300 K [Fig. 3(a)]. It is worth noting that the resistivity of CaCd$_2$As$_2$ is much smaller than SrCd$_2$As$_2$ ($\rho_{300K} \sim 1 * 10^4$ Ω mm and $\rho_{120K} \sim 1 * 10^7$ Ω mm).[21] It is consistent with the aforementioned scenario that shortened Cd/Mn–As bond lengths and optimized As–Zn/Mn–As bond angle within sublayers enhance intrasublayer Cd/Mn–As hybridization and in turn benefit conduction. On the other hand, ρ_{2K} of CaCd$_2$As$_2$ is 3 orders magnitude larger than all the Na-doped (Ca,Na)(Cd,Mn)$_2$As$_2$, indicating significantly increased carrier concentrations via Na doping. The scheme is further supported as shown in Fig. 3(a) by the decrease in resistivity of (Ca$_{1-x}$Na$_x$)(Cd$_{0.85}$Mn$_{0.15}$)$_2$As$_2$ with an increasing Na-doping level. In contrast, as shown in Fig. 3(b), resistivity of

(Ca$_{0.95}$Na$_{0.05}$)(Cd$_{1-y}$Mn$_y$)$_2$As$_2$ gradually increases with increasing Mn concentrations.

Figure 4(a) shows $\rho(T)$ curves for (Ca$_{0.95}$Na$_{0.05}$)(Cd$_{0.85}$Mn$_{0.15}$)$_2$As$_2$ under various fields. Negative magnetoresistance [MR = $\Delta\rho/\rho_0$ = $(\rho_H - \rho_0)/\rho_0$] is found below ~18 K consistent with T_C from magnetization data. Above 18 K, positive MR emerges. The consistency indicates that the negative MR is related to ferromagnetic ordering. In Fig. 4(b), MR does not saturate at H = 7 T and T = 2 K, where the spins are almost fully aligned according to the $M(H)$ curve. In (Ga,Mn)As and analog (Sr,Na)(Cd,Mn)$_2$As$_2$, the unsaturated MR is explained with giant splitting of the valence band. In order to understand such behavior, the negative magnetoresistance dates at 2 K are fitted with following equation:[24–26]

$$\Delta\rho/\rho_H = \Delta\sigma/\sigma = kB^{1/2} = -n_v e^2 C_0 \rho (eB\hbar)^{1/2}/(2\pi^2\hbar), \qquad (1)$$

where $C_0 \approx 0.605$, e is the elemental charge, $\hbar$ is the reduced Planck constant, and $1/2 \leq n_v \leq 2$ depending on the number of hole subbands contributing to the charge transport. The best fitting to Eq. (1) gives n_v = 0.62, close to that of (Sr,Na)(Cd,Mn)$_2$As$_2$. The maximum MR is ~15% at T = 2 K and H = 7 T. It is larger than analogs (Sr,Na)(Zn,Mn)$_2$As$_2$ and (Ca,Na)(Zn,Mn)$_2$As$_2$ as well as (Ba,K)(Zn,Mn)$_2$As$_2$ which has a much higher T_C.[10,27,28]

The carrier type of the parent phase CaCd$_2$As$_2$ and doped phase (Ca,Na)(Cd,Mn)$_2$As$_2$ is p-type. The hole concentration of these samples is about 10^{19}–10^{20} cm^{-3}. Figure 4(c) shows Hall resistivity [$\rho_{xy}(H)$] below and above T_C for (Ca$_{0.9}$Na$_{0.1}$)(Cd$_{0.85}$Mn$_{0.15}$)$_2$As$_2$ as a typical example. At T = 2 K, the clear anomalous Hall effect (AHE) is a strong evidence for intrinsic ferromagnetism in a DMS material. Carrier concentration calculated with linear $\rho_{xy}(H)$ at a high-field range is $n_p = 2.98 \times 10^{19}$ cm^{-3}. At 300 K, ρ_{xy} is proportional to field and we obtain $n_p = 5.38 \times 10^{19}$ cm^{-3}.

Considering key roles of local geometry of [Zn/MnAs]$_4$ tetrahedra to ferromagnetic interaction in BZA, we compare Cd/Mn–As bond lengths and As–Cd/Mn–As bond angles of CaCd$_2$As$_2$ and SrCd$_2$As$_2$ to seek microscopic insight into the origin of improved ferromagnetic ordering in CaCd$_2$As$_2$. For carrier-mediated ferromagnetism in DMS, itinerant carriers play an important role in ferromagnetic interaction.[29–38] Given the quasi-2D structure of CaCd$_2$As$_2$ and SrCd$_2$As$_2$, one can expect that carriers are more itinerant along the ab-plane than the c-axis. If one takes a close look at Cd$_2$As$_2$ planes, it is easy to find two sublayers within one CdAs plane [Fig. 1(a)]. It is reasonable to assume that intrasublayer component is more important than the intersublayer one to modify carrier mobility within the Cd$_2$As$_2$ plane. With the same doping levels, the sublayer of CaCd$_2$As$_2$ has shorter Cd/Mn–As bond length and more optimal As–Cd/Mn–As bond angles than that of SrCd$_2$As$_2$. As shown in Fig. 1(d), the (Ca$_{0.95}$Na$_{0.05}$)(Cd$_{0.95}$Mn$_{0.05}$)As$_2$ has the average Cd/Mn–As bond length of 2.700 Å and the average As–Cd/Mn–As bond angle within sublayers of 108.9° that is close to the ~109.47° for a nondistorted ideal tetrahedron.[18] On the other hand, in (Sr$_{0.95}$Na$_{0.05}$)(Cd$_{0.95}$Mn$_{0.05}$)As$_2$, the average Cd/Mn–As bond length is 2.712 Å and the average As–Cd/Mn–As bond angle is 113.6° that is apparently deviated from ~109.47°. The shortened Cd/Mn–As bond length will definitely increase Mn–As hybridization. Additionally, the ideal As–Cd/Mn–As bond angle will increase the overlap of Mn–As planar orbitals and guarantee the maximum strength of Mn–As hybridization, hence increasing the

(a)

(b)
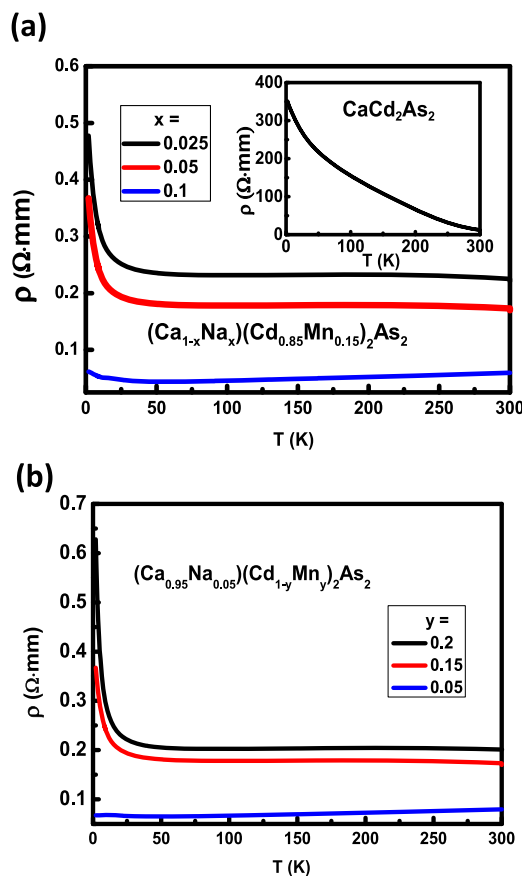
FIG. 3. Temperature dependent resistivity curves of (a) (Ca$_{1-x}$Na$_x$)(Cd$_{0.85}$Mn$_{0.15}$)$_2$As$_2$ (x = 0.025, 0.05, 0.1) and CaCd$_2$As$_2$ in the inset. (b) (Ca$_{0.95}$Na$_{0.05}$)(Cd$_{1-y}$Mn$_y$)$_2$As$_2$ (y = 0.05, 0.15, 0.2).
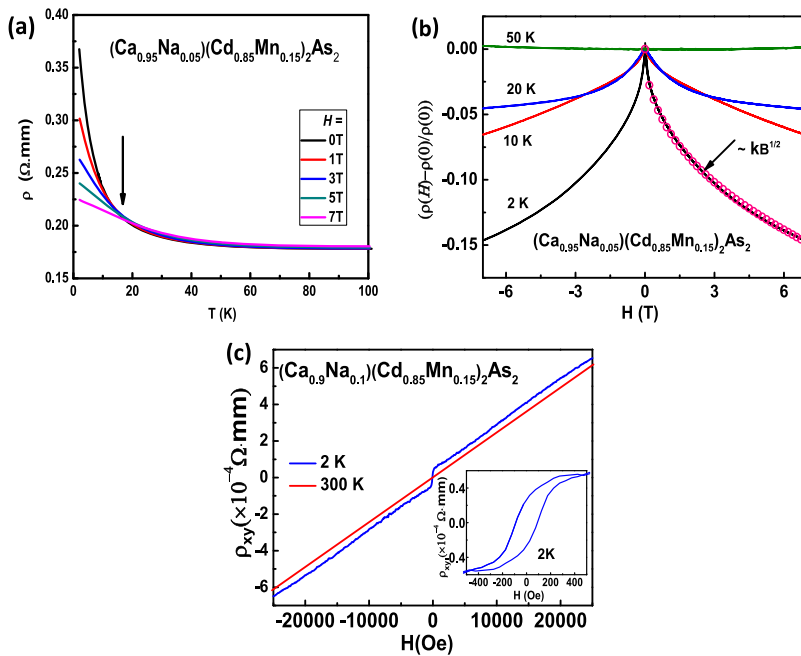
FIG. 4. (a) $\rho(T)$ curves of $(Ca_{0.95}Na_{0.05})(Cd_{0.85}Mn_{0.15})_2As_2$ under various fields. (b) Magnetoresistance curves of $(Ca_{0.95}Na_{0.05})(Cd_{0.85}Mn_{0.15})_2As_2$ measured in an external field up to 7 T at T = 2, 10, 20, and 50 K, respectively. The pink circles show the fitting result according to Eq. (1). (c) Hall effect measurement results for $(Ca_{0.9}Na_{0.1})(Cd_{0.85}Mn_{0.15})_2As_2$. The inset shows AHE and hysteresis loop in the low-field region.

ferromagnetic interactions. Previous studies of physical pressure-effects on "122" BZA indicated that shortened Zn/Mn–As bond length and optimized As–Zn/Mn–As bond angle (~109.47° for a regular tetrahedron) will enhance Cd/Mn–As hybridization.[18] In short, $(Ca,Na)(Cd,Mn)_2As_2$ has stronger intrasublayer Cd/Mn–As hybridization than that for $(Sr,Na)(Cd,Mn)_2As_2$. As a result, we found improved ferromagnetic ordering in $(Ca,Na)(Cd,Mn)_2As_2$. Consequently, it is reasonable to assume that more chemical pressure could further improve T_C within this system, e.g., replacing Ca with Mg.

We calculated the equation of state (EoS) equation with first-principles calculations with the plane augmented-wave (PW) pseudopotential method implemented in the VASP code[39] to build up relationship between cell volume and pressure [$P(V)$] of $SrCd_2As_2$ (Fig. S2). Based on the $P(V)$ curve, we estimate that an external pressure of 3.6 GPa can reduce cell volume of $SrCd_2As_2$ to 120.0 Å^3 (volume of $CaCd_2As_2$ at ambient pressure).

In summary, we successfully synthesized a new type of DMS, $(Ca,Na)(Cd,Mn)_2As_2$. The carriers and spins are introduced via (Ca,Na) and (Cd,Mn) substitutions independently. The Curie temperature of $(Ca,Na)(Cd,Mn)_2As_2$ is 50% higher than that of $(Sr,Na)(Cd,Mn)_2As_2$ due to the effects of chemical pressure, and the saturation moment is also enhanced dramatically. The significant improvement of ferromagnetism in $(Ca,Na)(Cd,Mn)_2As_2$ indicates the prospect to search for high temperature diluted magnetic semiconductors via proper chemical pressure.

See supplementary material for the PXRD pattern of $(Ca_{0.95}Na_{0.05})(Cd_{1-y}Mn_y)_2As_2$ (y = 0, 0.05, 0.1, 0.15, and 0.2) and the calculated $P(V)$ of $SrCd_2As_2$

REFERENCES

[1]I. Zutic, J. Fabian, and S. Das Sarma, Rev. Mod. Phys. **76**, 323 (2004).

[2]T. Jungwirth, J. Wunderlich, V. Novak, K. Olejnik, B. L. Gallagher, R. P. Campion, K. W. Edmonds, A. W. Rushforth, A. J. Ferguson, and P. Nemec, Rev. Mod. Phys. **86**, 855 (2014).

[3]H. Ohno, Science **281**, 951 (1998).

[4]N. T. Tu, P. N. Hai, L. D. Anh, and M. Tanaka, Appl. Phys. Lett. **108**, 192401 (2016).

[5]N. T. Tu, P. N. Hai, L. D. Anh, and M. Tanaka, Appl. Phys. Express **11**, 063005 (2018).

[6]N. T. Tu, P. N. Hai, L. D. Anh, and M. Tanaka, Appl. Phys. Lett. **112**, 122409 (2018).

[7]A. Hirohata, H. Sukegawa, H. Yanagihara, I. Zutic, T. Seki, S. Mizukami, and R. Swaminathan, IEEE Trans. Magn. **51**, 0800511 (2015).

[8]I. Zutic and T. Zhou, Sci. China: Phys., Mech. Astron. **61**, 067031 (2018).

[9]J. K. Glasbrenner, I. Zutic, and I. I. Mazin, Phys. Rev. B **90**, 140403 (2014).

[10]K. Zhao, Z. Deng, X. C. Wang, W. Han, J. L. Zhu, X. Li, Q. Q. Liu, R. C. Yu, T. Goko, B. Frandsen, L. Liu, F. Ning, Y. J. Uemura, H. Dabkowska, G. M. Luke, H. Luetkens, E. Morenzoni, S. R. Dunsiger, A. Senyshyn, P. Böni, and C. Q. Jin, Nat. Commun. **4**, 1442 (2013).

[11]K. Zhao, B. J. Chen, G. Q. Zhao, Z. Yuan, Q. Q. Liu, Z. Deng, J. L. Zhu, and C. Q. Jin, Chin. Sci. Bull. **59**, 2524 (2014).

[12]H. Ohno, D. Chiba, F. Matsukura, T. Omiya, E. Abe, T. Dietl, Y. Ohno, and K. Ohtani, Nature **408**, 944 (2000).

[13]M. Csontos, G. Mihaly, B. Janko, T. Wojtowicz, X. Liu, and J. K. Furdyna, Nat. Mater. **4**, 447 (2005).

[14] M. Almamouri, P. P. Edwards, C. Greaves, and M. Slaski, Nature **369**, 382 (1994).

[15] W. B. Gao, Q. Q. Liu, L. X. Yang, Y. Yu, F. Y. Li, C. Q. Jin, and S. Uchida, Phys. Rev. B **80**, 094523 (2009).

[16] S. Kasahara, T. Shibauchi, K. Hashimoto, K. Ikada, S. Tonegawa, R. Okazaki, H. Shishido, H. Ikeda, H. Takeya, K. Hirata, T. Terashima, and Y. Matsuda, Phys. Rev. B **81**, 184519 (2010).

[17] S. A. J. Kimber, A. Kreyssig, Y. Z. Zhang, H. O. Jeschke, R. Valenti, F. Yokaichiya, E. Colombier, J. Yan, T. C. Hansen, T. Chatterji, R. J. McQueeney, P. C. Canfield, A. I. Goldman, and D. N. Argyriou, Nat. Mater. **8**, 471 (2009).

[18] F. Sun, G. Q. Zhao, C. A. Escanhoela, B. J. Chen, R. H. Kou, Y. G. Wang, Y. M. Xiao, P. Chow, H. K. Mao, D. Haskel, W. G. Yang, and C. Q. Jin, Phys. Rev. B **95**, 094412 (2017).

[19] G. Q. Zhao, Z. Li, F. Sun, Z. Yuan, B. J. Chen, S. Yu, Y. Peng, Z. Deng, X. C. Wang, and C. Q. Jin, J. Phys.: Condens. Matter **30**, 254001 (2018).

[20] F. Sun, N. N. Li, B. J. Chen, Y. T. Jia, L. J. Zhang, W. M. Li, G. Q. Zhao, L. Y. Xing, G. Fabbris, Y. G. Wang, Z. Deng, Y. J. Uemura, H. K. Mao, D. Haskel, W. G. Yang, and C. Q. Jin, Phys. Rev. B **93**, 224403 (2016).

[21] B. J. Chen, Z. Deng, W. M. Li, M. R. Gao, Z. Li, G. Q. Zhao, S. Yu, X. C. Wang, Q. Q. Liu, and C. Q. Jin, J. Appl. Phys. **120**, 083902 (2016).

[22] P. Klufers and A. Mewis, Z. Naturforsch., B **32**, 753 (1977).

[23] X. Yang, Y. Li, P. Zhang, H. Jiang, Y. Luo, Q. Chen, C. Feng, C. Cao, J. Dai, T. Qian, G. Cao, and Z.-A. Xu, J. Appl. Phys. **114**, 223905 (2013).

[24] A. Kawabata, Solid State Commun. **34**, 431 (1980).

[25] T. Omiya, F. Matsukura, T. Dietl, Y. Ohno, T. Sakon, M. Motokawa, and H. Ohno, Physica E **7**, 976 (2000).

[26] F. Matsukura, M. Sawicki, T. Dietl, D. Chiba, and H. Ohno, Physica E **21**, 1032 (2004).

[27] B. J. Chen, K. Zhao, Z. Deng, W. Han, J. L. Zhu, X. C. Wang, Q. Q. Liu, B. Frandsen, L. Liu, S. Cheung, F. L. Ning, T. J. S. Munsie, T. Medina, G. M. Luke, J. P. Carlo, J. Munevar, Y. J. Uemura, and C. Q. Jin, Phys. Rev. B **90**, 155202 (2014).

[28] K. Zhao, B. J. Chen, Z. Deng, W. Han, G. Q. Zhao, J. L. Zhu, Q. Q. Liu, X. C. Wang, B. Frandsen, L. Liu, S. Cheung, F. L. Ning, T. J. S. Munsie, T. Medina, G. M. Luke, J. P. Carlo, J. Munevar, G. M. Zhang, Y. J. Uemura, and C. Q. Jin, J. Appl. Phys. **116**, 163906 (2014).

[29] Z. Deng, C. Q. Jin, Q. Q. Liu, X. C. Wang, J. L. Zhu, S. M. Feng, L. C. Chen, R. C. Yu, C. Arguello, T. Goko, F. L. Ning, J. S. Zhang, Y. Y. Wang, A. A. Aczel, T. Munsie, T. J. Williams, G. M. Luke, T. Kakeshita, S. Uchida, W. Higemoto, T. U. Ito, B. Gu, S. Maekawa, G. D. Morris, and Y. J. Uemura, Nat. Commun. **2**, 422 (2011).

[30] Z. Deng, K. Zhao, B. Gu, W. Han, J. L. Zhu, X. C. Wang, X. Li, Q. Q. Liu, R. C. Yu, T. Goko, B. Frandsen, L. Liu, J. S. Zhang, Y. Y. Wang, F. L. Ning, S. Maekawa, Y. J. Uemura, and C. Q. Jin, Phys. Rev. B **88**, 081203 (2013).

[31] R. Wang, Z. X. Huang, G. Q. Zhao, S. Yu, Z. Deng, C. Q. Jin, Q. J. Jia, Y. Chen, T. Y. Yang, X. M. Jiang, and L. X. Cao, AIP Adv. **7**, 045017 (2017).

[32] G. Q. Zhao, C. J. Lin, Z. Deng, G. X. Gu, S. Yu, X. C. Wang, Z. Z. Gong, Y. J. Uemera, Y. Q. Li, and C. Q. Jin, Sci. Rep. **7**, 14473 (2017).

[33] C. Ding, H. Y. Man, C. Qin, J. C. Lu, Y. L. Sun, Q. Wang, B. Q. Yu, C. M. Feng, T. Goko, C. J. Arguello, L. Liu, B. A. Frandsen, Y. J. Uemura, H. D. Wang, H. Luetkens, E. Morenzoni, W. Han, C. Q. Jin, T. Munsie, T. J. Williams, R. M. D'Ortenzio, T. Medina, G. M. Luke, T. Imai, and F. L. Ning, Phys. Rev. B **88**, 041102 (2013).

[34] W. Han, K. Zhao, X. C. Wang, Q. Q. Liu, F. L. Ning, Z. Deng, Y. Liu, J. L. Zhu, C. Ding, H. Y. Man, and C. Q. Jin, Sci. China: Phys., Mech. Astron. **56**, 2026 (2013).

[35] H. Y. Man, S. L. Guo, Y. Sui, Y. Guo, B. Chen, H. D. Wang, C. Ding, and F. L. Ning, Sci. Rep. **5**, 15507 (2015).

[36] F. Sun, C. Xu, S. Yu, B. J. Chen, G. Q. Zhao, Z. Deng, W. G. Yang, and C. Q. Jin, Chin. Phys. Lett. **34**, 067501 (2017).

[37] B. A. Frandsen, Z. Z. Gong, M. W. Terban, S. Banerjee, B. J. Chen, C. Q. Jin, M. Feygenson, Y. J. Uemura, and S. J. L. Billinge, Phys. Rev. B **94**, 094102 (2016).

[38] S. C. Erwin and I. Zutic, Nat. Mater. **3**, 410 (2004).

[39] G. Kresse and D. Joubert, Phys. Rev. B **59**(3), 1758 (1999).